Materials Science and Engineering C 40 (2014) 109–120

Contents lists available at ScienceDirect

Materials Science and Engineering C

journal homepage: www.elsevier.com/locate/msec

Computer-assisted electrochemical fabrication of a highly selective and sensitive amperometric nitrite sensor based on surface decoration of electrochemically reduced graphene oxide nanosheets with CoNi bimetallic alloy nanoparticles

Mohammad-Bagher Gholivand [a,*], Ali R. Jalalvand [a,b], Hector C. Goicoechea [b]

[a] Faculty of Chemistry, Razi University, Kermanshah 671496734, Iran
[b] Laboratorio de Desarrollo Analítico y Quimiometría (LADAQ), Cátedra de Química Analítica I, Universidad Nacional del Litoral, Ciudad Universitaria, CC 242 (S3000ZAA), Santa Fe, Argentina

ARTICLE INFO

Article history:
Received 4 November 2013
Received in revised form 1 March 2014
Accepted 18 March 2014
Available online 26 March 2014

Keywords:
Nitrite sensor
Electrochemical fabrication
Experimental design
Simultaneous optimization

ABSTRACT

For the first time, a novel, robust and very attractive statistical experimental design (ED) using minimum-run equireplicated resolution IV factorial design (Min-Run Res IV FD) coupled with face centered central composite design (FCCCD) and Derringer's desirability function (DF) was developed to fabricate a highly selective and sensitive amperometric nitrite sensor based on electrodeposition of CoNi bimetallic alloy nanoparticles (NPs) on electrochemically reduced graphene oxide (ERGO) nanosheets. The modifications were characterized by cyclic voltammetry (CV), electrochemical impedance spectroscopy (EIS), energy dispersive X-ray spectroscopic (EDS), scanning electron microscopy (SEM) techniques. The CoNi bimetallic alloy NPs were characterized using digital image processing (DIP) for particle counting (density estimation) and average diameter measurement. Under the identified optimal conditions, the novel sensor detects nitrite in concentration ranges of 0.1–30.0 μM and 30.0–330.0 μM with a limit of detection (LOD) of 0.05 μM. This sensor selectively detects nitrite even in the presence of high concentration of common ions and biological interferents therefore, we found that the sensor is highly selective. The sensor also demonstrated an excellent operational stability and good antifouling properties. The proposed sensor was used to the determination of nitrite in several foodstuff and water samples.

1. Introduction

Nitrite as a typical inorganic pollutant, has caused serious hazards to public health and the environment, and its anthropogenic sources are wastes from fertilizers [1]. Nitrite promotes the irreversible oxidization of hemoglobin to methemoglobin and reduces the blood capacity to transport oxygen [2]. In addition, it can react with amines to form N-nitrosamines, many of which are known to be carcinogens [3,4]. Hence, selective and sensitive determination of nitrite has become important. There are many analytical technologies for nitrite detection, mainly containing spectrophotometry [5,6], chromatography [7,8], capillary electrophoresis chemiluminescence [9] and electrochemistry [10–13]. Electrochemical techniques have been proved to be one of the most advantageous ways in the determination of nitrite.

Graphene is a single-atom-thick planar sheet of hexagonally arrayed sp^2-bonded carbon atoms packed in a 2-D honeycomb crystal lattice [14]. Many desirable properties of graphene have been revealed such as high surface-to-volume ratio, large surface area, high electrocatalytic activity, fast electron transfer, low cost, robust mechanical properties, flexibility and outstanding conductivity [15], making it a promising material for applications in electronics/optoelectronics [16], sensors [17], composites [15], batteries [18] and supercapacitors [19]. However, as the existence of residual defects in graphene can exert a significant influence on its electronic properties, efficient reduction of oxygenated species in graphene is necessary to prevent possible unwanted reactions and electrostatic adsorptions. Numerous studies have focused on the synthesis and applications of graphene inorganic nanocomposite materials [16,20]. However, undesirable excessive reducing agents used in

Abbreviations: ED, experimental design; Min-Run Res IV FD, minimum-run equireplicated resolution IV factorial design; FCCCD, face centered central composite design; DF, Derringer's desirability function; NPs, nanoparticles; ERGO, electrochemically reduced graphene oxide; GCE, glassy carbon electrode; CV, cyclic voltammetry; LOD, limit of detection; DIP, digital image processing; EIS, electrochemical impedance spectroscopy; SEM, scanning electron microscopy; EDS, energy dispersive X-ray spectroscopy; PSDs, particle size distributions; COFAT, changing one factor at a time; ANOVA, analysis of variance; LOF, lack of fit; GO, graphene oxide; RSM, response surface methodology; PBS, phosphate buffer solution; 3-FFD, three-level full-factorial design; CCD, central composite design; BBD, Box–Behnken design; DMD, Doehlert Matrix design; RSD, relative standard deviation.

* Corresponding author. Tel.: +98 831 4274557; fax: +98 831 4274559.
E-mail addresses: mbgholivand2013@gmail.com, mbgholivand@yahoo.com (M.-B. Gholivand).

http://dx.doi.org/10.1016/j.msec.2014.03.044
0928-4931/© 2014 Published by Elsevier B.V.

these methods both increase the cost in mass production and possibly remain and contaminate the synthesized materials. Meanwhile, oxygen-containing functional groups (−OH, C−O−C in the basal plane and −COOH on the edges) in graphene cannot be completely eliminated by chemical reduction [21]. Therefore, it is of great interest to look for a simple and environmentally friendly approach for synthesis of graphene sheet-NPs composites. Electrochemical methods are useful in reduction of graphene oxide (GO), strictly speaking an insulator, to eliminate oxygenated defect sites and improve its electronic properties [22].

Heterogeneous bimetallic alloy NPs have recently received much attention as electrocatalysts with enhanced activities and electrochemical reversibility for redox reactions. These bimetallic alloys can retain the functional properties of each component and possibly offer synergistic effects via cooperative interactions, resulting in important features such as increased surface area, enhanced electrocatalytic activity, improved biocompatibility, promoted electron transfer, and better invulnerability against intermediate species [23]. Owing to these advantages of bimetallic alloy NPs, our interest was shifted to develop CoNi bimetallic alloy nanoparticles for application in electrochemical sensing with appropriate characteristics such as high sensitivity, wide linear range, better selectivity, repeatability and reproducibility. Electrodeposition is the most controllable and robust technique for the synthesis of metal NPs, in which the size, density, composition of alloys and even the shape of NPs can be well-controlled by electrochemical conditions of the procedure, concentration, and composition of metal precursor solutions [24]. Herein, GO was firstly electrochemically reduced at a glassy carbon electrode (GCE) with a process free of reducing agents. The electrodeposited CoNi bimetallic alloy NPs were then used to modify the ERGO.

The sizes of NPs are commonly linked to their physicochemical properties [25], with different crystal nucleation and growth processes giving rise to different particle size distributions (PSDs). In order to provide statistically meaningful size distributions from SEM images, many particles should be analyzed. Image segmentation is an essential preliminary step in most automated pattern recognition and scene analysis problems. Segmentation is used to subdivide an image into its constituent regions, and its accuracy determines the eventual success or failure of computerized analysis procedures. Manual segmentation of SEM images can be time-consuming and subjective because, in most cases, it is difficult to analyze an image locally to obtain only the desired information from the particles. In order to address these issues, we have used DIP based on a semi-automatic approach and adaptive local thresholding that allows particles to be detected and characterized with greater accuracy than using more conventional methods, in which a global threshold is used.

The method of changing one factor at a time (COFAT) to investigate the outcome of an experiment most likely dates back to the beginnings of systematic scientific research. This method is time consuming and requires a number of experiments to determine optimum levels, which are unreliable. Statistical ED is a very useful tool for this purpose as it provides statistical models, which help in understanding the interactions among the parameters that have been optimized [26,27].

A widely used methodology for developing, improving and optimizing systems, the so-called response surface methodology (RSM), consists of the following general phases: 1) Screening: experiments are designed with the purpose of discovering the vital few control variables that cause statistically significant effects of practical importance for the goal of the study; 2) Modeling: experiments are designed with the purpose of modeling the quality of interest response as a function of control variables; 3) Optimization: response model is analyzed to determine the variable settings at which optimum conditions of system property are achieved. This methodology has inherent sequential experimentation strategy that, if the technical and non-technical issues in the experimental phases are properly managed, leads to a high level of system knowledge. For an understanding of the assumptions and conditions necessary to successfully apply RSM the reader is referred to Refs. [28–30].

Literature survey revealed that graphene has catalytic effects on oxidation of nitrite [31]. Here, we wish to further modify graphene with CoNi bimetallic alloy NPs and see its performance towards oxidation of nitrite. The main aim of the present work was to develop, optimize and validate a novel, highly selective and sensitive amperometric nitrite sensor with the aid of ED. We have coupled computational approaches with experimental ones to introduce a very attractive study which is unique among the methods reported in the literature for constructing the electrochemical sensors. To the best of our knowledge, this work is the first report on using an advanced optimization procedure at the field of electrochemistry and it will surely be a great base for more interesting studies in near future.

2. Experimental and theoretical backgrounds

2.1. Chemicals and solutions

All chemicals used in this study were of analytical grade from Merck (otherwise those stated) and used without further purification. Graphite flakes (150.0 μm flakes) were purchased from Sigma-Aldrich, USA. Phosphate buffer solutions (PBS, 0.05 M) at various pH values were prepared using Na_2HPO_4, and NaH_2PO_4. Griess reagent was prepared by mixing equal volumes of solutions of α-napthylamine (0.1 g dissolved in 100.0 mL of double-distilled water (ddH_2O)) and sulphanylamide (1.0 g of the reactant, 5.9 mL of concentrated phosphoric acid solution and dilution to 100.0 mL with ddH_2O). Absorbance measurements were performed at 534.0 nm. The ddH_2O was used throughout the study and high purity N_2 was applied for deaeration.

2.2. Apparatus and softwares

Electrochemical experiments were performed using a μ-Autolab TYPE III, Eco Chemie BV, Netherlands, equipped with PSTA 20 model and driven by NOVA 1.8 software. A conventional three-electrode cell was used with a saturated Ag/AgCl as reference electrode, a Pt wire as counter electrode and a bare (with an area of 0.017 cm^2) or modified GCE as working electrode. Before the modifications, the GCE was carefully polished on a fine microcloth successively with 0.3 and 0.05 μm

Table 1
The studied variables and responses.

Variables	Range and levels		Responses
	−1	+1	
(*A*) Volume of GO.	0.5	4 (μL)	(R_1) Peak current (A)
(*B*) Rate of scanning potential for reducing GO.	50	100 (mV s^{-1})	(R_2) Peak potential (V)
(*C*) No. of cycles applied for reducing GO.	25	125 (cycles)	
(*D*) pH of the PBS used for reducing GO.	4	8 (pH)	
(*E*) No. of cycles applied for the electrodeposition of NPs.	10	50 (cycles)	
(*F*) Rate of scanning potential for electrodeposition of NPs.	50	100 (mV s^{-1})	
(*G*) [Co]/[Ni]	0.33	3	
(*H*) pH of the PBS containing nitrite.	4	8 (pH)	

Table 2
The Min Run Res IV FD and experimental results.

Experiment	Variables' levels								Responses	
	A	*B*	*C*	*D*	*E*	*F*	*G*	*H*	R_1 (A)	R_2 (V)
1	4	100	125	6	10	50	0.33	8	0.0000575	0.88
2	4	100	25	3	50	50	0.33	4	0.0000536	0.82
3	0.5	100	25	6	50	100	0.33	8	0.0000535	0.80
4	4	50	125	3	50	100	3	4	0.0000645	0.74
5	0.5	100	25	6	10	50	3	4	0.0000488	0.93
6	4	100	25	3	10	100	3	8	0.0000476	0.85
7	2.25	75	75	4	30	75	1.67	6	0.0000833	0.80
8	4	50	125	3	10	50	3	4	0.0000731	0.83
9	0.5	100	125	3	10	100	0.33	4	0.0000638	0.92
10	4	50	25	6	50	50	3	8	0.0000439	0.78
11	4	100	125	6	50	100	3	4	0.0000664	0.74
12	0.5	100	125	3	50	50	3	8	0.0000568	0.76
13	0.5	100	25	6	10	50	0.33	8	0.0000412	0.93
14	0.5	50	25	3	50	100	3	4	0.0000475	0.73
15	4	50	25	6	10	100	0.33	4	0.0000484	0.87
16	0.5	50	125	6	10	100	3	8	0.0000606	0.79
17	4	50	125	3	50	100	0.33	8	0.0000523	0.80
18	2.25	75	75	4.5	30	75	1.67	6	0.0000856	0.79
19	0.5	50	125	6	50	50	0.33	4	0.0000561	0.81
20	0.5	50	25	3	10	50	0.33	8	0.0000381	0.91

alumina slurry (Beuhler) until a mirror-shine surface was obtained, and then rinsed with ddH_2O. A sonication step was performed consecutively in ethanol and ddH_2O and GCE was then dried at room temperature. The UVvis spectrophotometric measurements were performed on an Agilent 8453 UVvis Diode-Array spectrophotometer controlled by the Agilent UVvis ChemStation software. A JENWAY-3345 pH-meter equipped with a combined glass electrode was used to pH measurements. The SEM experiment was made on a KYKY-EM 3200 scanning electron microscope. Energy dispersive X-ray spectroscopic (EDS) detecting unit was used for elemental analysis. The EIS was carried out using the same three-electrode configuration above on the mentioned Autolab in a supporting electrolyte solution of 1.0 M KCl containing equimolar $[Fe(CN)_6]^{4-/3-}$ in a frequency range from 0.1 Hz to 100.0 kHz. The fit and simulation of equivalent circuit were analyzed with FRA software. A licensed Design Expert software (Version 8.0) was purchased from Stat-Ease and applied for designing of experiments. All the recorded electrochemical data was smoothed, when necessary, and converted to data matrices by the use of several home-made mfiles in MATLAB environment (Version 7.14, MathWorks, Inc.). The asymmetric least squares splines regression (AsLSSR) algorithm was applied for baseline correction in MATLAB environment. The DIP was carried out on the SEM image of the surface of the modified electrode using a MATLAB code and an adaptive thresholding algorithm. All computations were run on a DELL XPS laptop (L502X) with Intel Core i7-2630QM 2.0 GHz, 8 GB of RAM and Windows 7–64 as its operating system.

2.3. Synthesis of GO

The GO was synthesized using a modified Hummer's method [32, 33]. Typically, 3.0 g graphite flakes, 2.5 g $K_2S_2O_8$ and 2.5 g P_2O_5 were added to 12.0 mL concentrated H_2SO_4 solution and reacted at 80.0 °C for 4.5 h. After graphite oxidation, the mixture was diluted with 500.0 mL ddH_2O and kept at 80.0 °C for another 12.0 h. The resulting solution was then filtered, washed with ddH_2O and left overnight for drying at room temperature, before re-dispersing in 120.0 mL concentrated H_2SO_4 with successive addition of 15.0 g $KMnO_4$ at temperature kept below 20.0 °C under stirring. The mixture was left stirred at 40.0 °C for 0.5 h and 90.0 °C for 1.5 h, followed by drop-wise addition of 250.0 mL ddH_2O, incubation at 105.0 °C for 25.0 min and stirring at room temperature for 2.0 h. 700 mL ddH_2O and 20.0 mL 30.0% (w/w) H_2O_2 were added to terminate the reaction. The resulting products were then filtered, washed with 3.0 M HCl solution, and repeatedly washed with water until the pH value of filtrate was neutral. It was further purified by dialysis for one week to remove residual salts, acids and metal species and was re-suspended by ultrasonication in water to obtain a homogeneous GO solution.

Table 3
Face centered central composite design and experimental results.

Experiment	Variable levels					Responses	
	C	*E*	*F*	*G*	*H*	R_1 (A)	R_2 (V)
1	25	50	50	0.33	8	0.0001310	0.71
2	25	10	100	3	4	0.0000835	0.73
3	75	30	75	1.665	6	0.0000723	0.71
4	125	50	100	3	4	0.0001200	0.74
5	125	10	100	3	8	0.0001330	0.70
6	125	10	100	0.33	8	0.0000867	0.72
7[a]	75	30	75	1.665	6	0.0000893	0.83
8	25	10	50	0.33	8	0.0001170	0.72
9	25	10	100	0.33	8	0.0000893	0.70
10	75	30	75	0.33	6	0.0001170	0.72
11	125	50	50	0.33	4	0.0000317	0.72
12	25	50	50	0.33	4	0.0000346	0.75
13	25	50	100	0.33	4	0.0000273	0.73
14	75	30	75	3	6	0.0000904	0.71
15	125	50	50	0.33	8	0.0000821	0.70
16	125	50	100	3	8	0.0000860	0.70
17	25	10	100	3	8	0.0000489	0.69
18	75	30	75	1.665	6	0.0000939	0.71
19	125	10	50	0.33	8	0.0000900	0.69
20	125	30	75	1.665	6	0.0000757	0.72
21	25	10	50	3	8	0.0000918	0.71
22	25	10	50	0.33	4	0.0000170	0.77
23	75	30	75	1.665	8	0.0000785	0.70
24	25	50	100	3	8	0.0000621	0.70
25	75	30	100	1.665	6	0.0000700	0.70
26	25	50	50	3	4	0.0000192	0.73
27	125	50	100	0.33	4	0.0000163	0.76
28	75	30	75	1.665	4	0.0000104	0.74
29	75	30	50	1.665	6	0.0000329	0.72
30	125	10	100	3	4	0.0001310	0.73
31	25	50	100	3	4	0.0000358	0.74
32	125	50	50	3	8	0.0000681	0.71
33	75	30	75	1.665	6	0.0000479	0.72
34	25	30	75	1.665	6	0.0000017	0.71
35	25	50	100	0.33	8	0.0000862	0.69
36	75	30	75	1.665	6	0.0000422	0.70
37	25	10	50	3	4	0.0000299	0.71
38	125	50	50	3	4	0.0000285	0.71
39	75	30	75	1.665	6	0.0000283	0.69
40	75	10	75	1.665	6	0.0000313	0.70
41	125	10	50	0.33	4	0.0000421	0.74
42	125	10	50	3	8	0.0000696	0.70
43	125	10	50	3	4	0.0000281	0.72
44	75	30	75	1.665	6	0.0000250	0.71
45	25	10	100	0.33	4	0.0000287	0.74
46	25	50	50	3	8	0.0000595	0.71
47	75	50	75	1.665	6	0.0000615	0.69
48	125	10	100	0.33	4	0.0000268	0.75
49	125	50	100	0.33	8	0.0000500	0.69
50	75	30	75	1.665	6	0.0000123	0.69

[a] Outlying.

For preparing the novel sensor according to the computationally designed experiments we applied the following procedure: a distinct volume (variable *A* (μL), Table 1) of 1.0 mg mL^{-1} of the above-prepared GO solution was cast on the pretreated bare GCE surface and dried in ambient condition. The electrochemical reduction of GO on GCE was conducted by repetitive CV with scanning from 0 V to −1.5 V at a distinct scan rate (variable *B* (mV s^{-1}), Table 1) for a distinct number of cycles (variable *C*, Table 1) in deaerated 0.05 M PBS with a distinct pH (variable *D*, Table 1). The ERGO/GCE was then rinsed with ddH_2O and dried at room temperature. The modification of ERGO with CoNi bimetallic alloy NPs with a distinct ratio (variable *G*, Table 1) was achieved by electrodeposition under repetitive CV with scanning from 0 V to −1.5 V at a distinct scan rate (variable *F* (mV s^{-1}), Table 1) for a distinct

number of cycles (variable *E*, Table 1). Finally, by putting the constructed sensor in a nitrite solution with a distinct pH (variable *H*, Table 1) the CV response related to oxidation of nitrite was recorded. The studied responses were peak current (R_1) and peak potential (R_2) of nitrite cyclic voltammogram (Table 1).

2.4. Preparation of the real samples

To evaluate the accuracy and applicability of the proposed methodology, the determination of nitrite in several real samples, i.e., Damavand mineral water (Damavand Co., Tehran, Iran), hot dog sausage (Bisetoon Co., Kermanshah, Iran), mortadella salami, (Bisetoon Co., Kermanshah, Iran) and feta white cheese (Guilan Pegah Dairy Co., Guilan, Iran) was performed. The extraction of nitrite from hot dog sausage, mortadella salami, and feta white cheese samples (weights of samples taken were 50.0 g, 50.0 g and 30.0 g, respectively) was accomplished by leaving a certain amount of crushed samples in deionized water at 70.0 °C under stirring for 10.0 min and further filtering of the remaining liquid. No preparation was required for mineral water sample.

2.5. Baseline correction

Baseline correction has been considered as a critical step for enhancing the signals and reducing the complexity of the analytical data [34]. Considering this aim, we used the method proposed by Eilers et al. [35] for background elimination in two-dimensional signals based on asymmetric least squares splines regression approach. In the asymmetric least squares method [36] the following cost function is minimized:

$$Q = \sum_i \upsilon_i (y_i - f_i)^2 + \lambda \sum_i \left(\Delta^2 f_i\right)^2 \quad (1)$$

Table 4
The results of ANOVA obtained by Min Run Res IV FD.

	SS	d.f.[a]	MS[b]	*F*-value	*P*-value
R_1					
Model	1.096×10^{-9}	2	5.482×10^{-10}	4.61	0.0251
C	8.187×10^{-10}	1	8.187×10^{-10}	6.89	0.0178
H	1.791×10^{-10}	1	1.791×10^{-10}	1.51	0.0236
Residual	2.021×10^{-9}	17			
			1.189×10^{-10}		
LOF[c]	2.019×10^{-9}	16	1.262×10^{-10}	47.7	0.1133
Pure error	2.645×10^{-12}	1	2.645×10^{-12}		
Total SS[d]	3.11×10^{-9}	19			
$R^2 = 0.8676$[e]					
Adj-$R^2 = 0.8392$[f]					
Pred-$R^2 = 0.7744$[g]					
R_2					
Model	0.065	3	0.022	26.47	<0.0001
E	0.039	1	0.039	47.71	<0.0001
F	3.782×10^{-3}	1	3.782×10^{-3}	4.61	0.0475
G	0.012	1	0.012	14.4	0.0016
Residual	0.013	16	8.203×10^{-4}		
LOF	0.013	15	8.717×10^{-4}	17.43	0.186
Pure error	5.000×10^{-5}	1	5.000×10^{-5}		
Total SS	0.078	19			
$R^2 = 0.9486$					
Adj-$R^2 = 0.9206$					
Pred-$R^2 = 0.8858$					

[a] Degrees of freedom.
[b] Mean square.
[c] Lack of fit.
[d] Sum of squares.
[e] Determination coefficient.
[f] Adjusted R^2.
[g] Predicted R^2.

where *y* is the experimental signal, *f* is a smooth approximation of baseline trend (*y*), Δ is the derivative of *f*, i denotes successive values of the signal, the positive parameter λ is a regularization parameter that weigh the second term and υ are weights. The positive deviations from the estimated baseline (peaks) have low υ values while the negative deviations (baseline) obtain high υ values. In the multidimensional extension of baseline correction method, Eilers et al. proposed the splines-based approach to smoothing instrumental signal (the penalty term in Eq. 1). Details of the implementation of the mentioned method can be found in the literature [35].

2.6. Statistical experimental design

2.6.1. Min-Run Res IV FD

In the presence of factors' interactions, only designs of resolution IV FD or higher can ensure accurate screening [37]. The methodology of Min-Run Res IV FD is a powerful and useful tool in rapidly searching key variables from a multivariable system. If we are limited by time, materials, or other experimental resources, in most cases Min-Run Res IV FD offers savings in runs over the equivalent standard two-level fractional factorial design [37].

A Min-Run Res IV FD was carried out to evaluate the effect of the eight variables (Table 1) and their interactions on R_1 and R_2. The levels of the variables were chosen based on previous works reported in literatures and our experiments. Here, an experimental matrix containing 20.0 runs was designed and employed (Table 2). The experiments were performed in a randomized order to assure the independence of the results and minimizing the effects of uncontrolled factors.

2.6.2. Selection of the optimization design

Among Response-surface designs with a symmetrical experimental domain, the following can be considered: three-level full-factorial (3-FFD), central composite (CCD), Box–Behnken (BBD), and Doehlert Matrix (DMD) designs [38].

The CCD is defined by the following polynomial model:

$$y = \beta_0 + \sum_{i=1}^{k} \beta_i x_i + \sum_{i=1}^{k} \beta_{ii} x_i^2 + \sum_{1 \neq j}^{k} \beta_{ij} x_i x_j + \varepsilon \quad (2)$$

where *y* is the dependent variable (Response); β_0 is the constant term, β_i, β_{ii} and β_{ij} represent the coefficients of the first order terms, quadratic terms and interaction terms respectively. The ε is residual associated to the experiments and *k* is the number of variables.

The CCD includes: two-level factorial design points (Fp), axial or star points (Sp) and central points (Cp). The Sp has all of the factors set to 0, except one factor which has the value $\pm\alpha$. The value of α determines the location of the Sp in the CCD and usually varies from 1 to $\sqrt{k}$. In order to model the responses with the significant variables a FCCCD which is considered to be 1 in α, was carried out in this study. The total number of design points needed (*N*) is determined by the following equation:

$$N = 2^k + 2\,k + C_P. \quad 3$$

Making replicates at the center point has two main objectives: to provide a measure of pure error, i.e., the error to be expected in the response if the experiment is repeated starting from scratch, and to stabilize the variance of the predicted response in the design region. Here, an experimental matrix was designed and employed (Table 3). The experiments were performed in a randomized order to assure the independence of the results, minimizing the effects of uncontrolled factors. Then, the previously commented responses were evaluated.

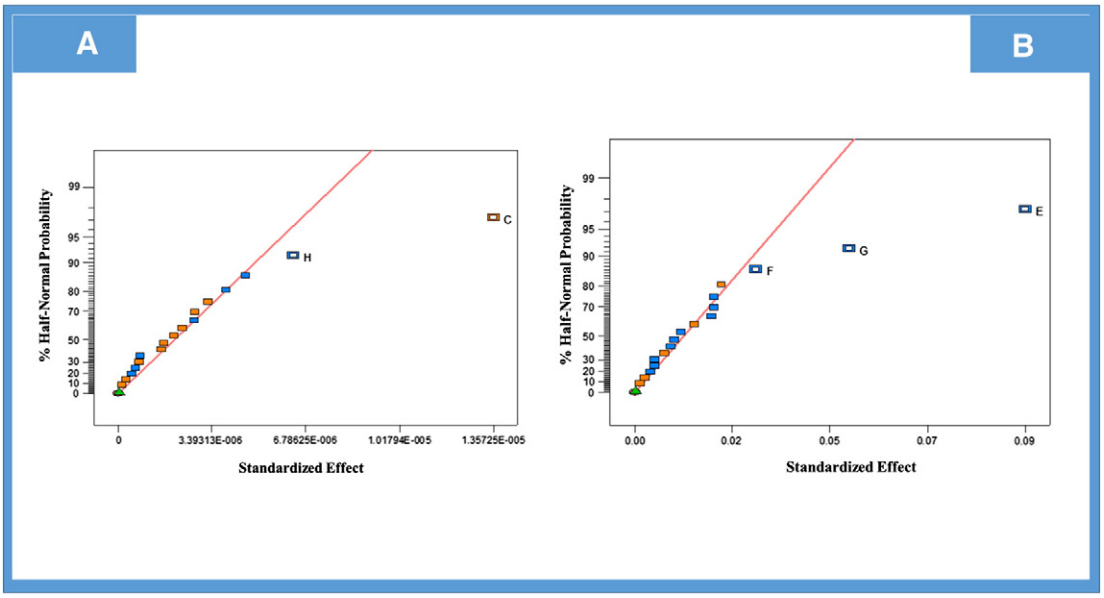

Fig. 1. The half-normal plots of effects of variables on (A) R_1 and (B) R_2.

2.6.3. Derringer's desirability function

The DF includes the researcher's priorities and desires on building the optimization procedure. Its application involves creating a function for each individual response (d_i) and finally obtaining a global function D that should be maximized or minimized choosing the best conditions of the designed variables. The latter function varies from 0 (totally undesirable value) to 1 (all responses are in a desirable range simultaneously), and can be defined by Eq. (4):

$$D = \left(d_1^{r_1} \times d_2^{r_2} \times \ldots \times d_m^{r_m}\right)^{\frac{1}{\sum r_j}} = \left(\prod_{j=1}^{m} d_j^{r_1}\right)^{\frac{1}{\sum r_j}} \quad (4)$$

where d_1,..., d_m correspond to the individual desirability functions for each response being optimized, m is the number of responses, and r is the relative importance of each response [39]. Remarkably, though this methodology presents considerable advantages in chemical analyses, some applications can be found in the literature [39–43].

2.7. Digital image processing

The DIP was carried out on the SEM image of the surface of the modified electrode using a MATLAB code and an adaptive thresholding algorithm. The contrast of the SEM images was inverted in order to display darker particles on a brighter background, calibrated and converted to bmp format suitable for further DIP. The program was designed with an interactive user interface, to allow squares with sizes selected by the user to be dragged to selected positions on the image in sequence and segmented using Otsu's method. The automated steps include: (1) thresholding each sub-image (the output from this procedure is a binary image), (2) opening (dilation plus erosion pixel-by-pixel with a chosen kernel size) and (3), combination and analysis of the processed

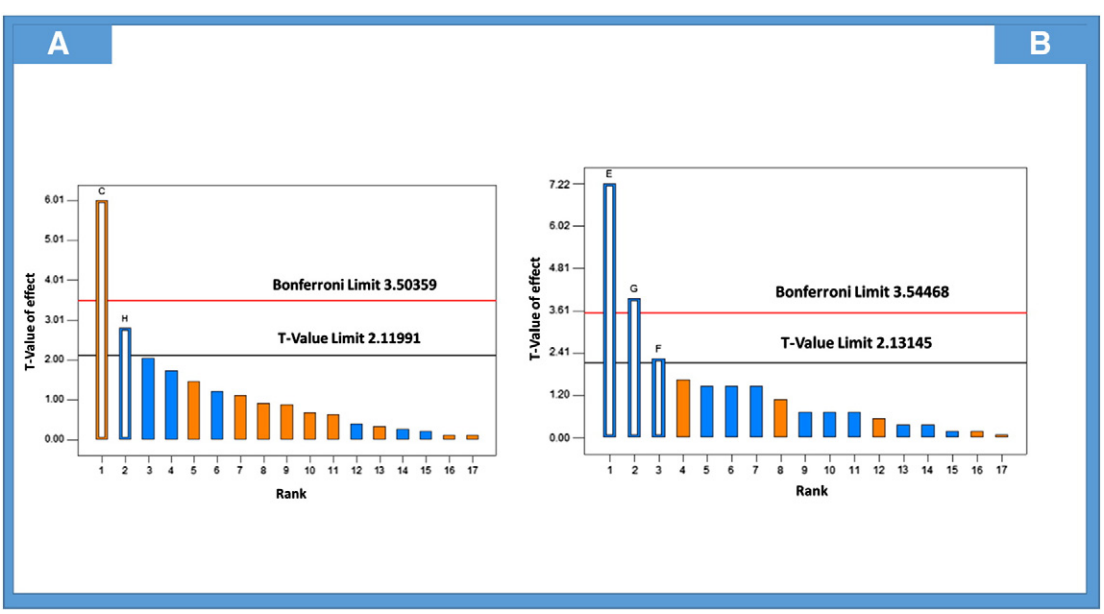

Fig. 2. The Pareto chart plots representing the size of variables' effects on (A) R_1 and (B) R_2.

Table 5
The results of ANOVA obtained by FCCCD.

	SS	d.f.[a]	MS[b]	*F*-value	*P*-value
R_1					
Model	1.493×10^{-4}	8	1.866×10^{-5}	5.58	<0.0001
C	7.175×10^{-6}	1	7.175×10^{-6}	2.14	0.1507
F	5.489×10^{-6}	1	5.489×10^{-6}	1.64	0.2074
G	8.473×10^{-7}	1	8.473×10^{-7}	0.25	0.6174
H	7.333×10^{-5}	1	7.333×10^{-5}	21.92	<0.0001
FG	1.349×10^{-5}	1	1.349×10^{-5}	4.03	0.0513
GH	1.799×10^{-5}	1	1.799×10^{-5}	5.38	0.0255
C^2	1.845×10^{-5}	1	1.845×10^{-5}	5.38	0.0237
G^2	3.080×10^{-5}	1	3.080×10^{-5}	9.21	0.0042
Residual	1.371×10^{-4}	41	3.345×10^{-6}		
LOF[c]	8.793×10^{-5}	34	2.586×10^{-6}	0.37	0.9763
Pure error	4.921×10^{-5}	7	7.029×10^{-6}		
Total SS[d]	2.864×10^{-4}	49			
$R^2 = 0.8435$[e]					
Adj-$R^2 = 0.8167$[f]					
Pred-$R^2 = 0.7546$[g]					
R_1					
Model	1.493×10^{-4}	8	1.866×10^{-5}	5.58	<0.0001
C	7.175×10^{-6}	1	7.175×10^{-6}	2.14	0.1507
F	5.489×10^{-6}	1	5.489×10^{-6}	1.64	0.2074
G	8.473×10^{-7}	1	8.473×10^{-7}	0.25	0.6174
H	7.333×10^{-5}	1	7.333×10^{-5}	21.92	<0.0001
FG	1.349×10^{-5}	1	1.349×10^{-5}	4.03	0.0513
GH	1.799×10^{-5}	1	1.799×10^{-5}	5.38	0.0255
C^2	1.845×10^{-5}	1	1.845×10^{-5}	5.38	0.0237
G^2	3.080×10^{-5}	1	3.080×10^{-5}	9.21	0.0042
Residual	1.371×10^{-4}	41	3.345×10^{-6}		
LOF[c]	8.793×10^{-5}	34	2.586×10^{-6}	0.37	0.9763
Pure error	4.921×10^{-5}	7	7.029×10^{-6}		
Total SS[d]	2.864×10^{-4}	49			
$R^2 = 0.8435$[e]					
Adj-$R^2 = 0.8167$[f]					
Pred-$R^2 = 0.7546$[g]					

[a] Degrees of freedom.
[b] Mean square.
[c] Lack of fit.
[d] Sum of squares.
[e] Determination coefficient.
[f] Adjusted R^2.
[g] Predicted R^2.

sub-images. This semiautomatic approach combining interactive selection of regions of interest with automated segmentation and analysis fully exploits the concept of adaptive thresholding, allowing the refinement of the results obtained using a fully automatic division of the images.

3. Results and discussion

3.1. Screening by Min-Run Res IV FD

Table 2 describes a Min-Run Res IV FD on eight variables which have been screened for evaluating their effects on R_1 and R_2. Table 4 shows the results of analysis of variance (ANOVA) for R_1 and R_2.

According to the results of ANOVA for R_1 (Table 4), the model *F*-value of 4.61 implies that the model is significant and there is only a 2.51% chance that a large *F*-value of 4.61 could occur due to noise. A *p*-value is a measure of how much evidence one has against the null hypothesis and evidence against null hypothesis is more for smaller *p*-value. A *p*-value of 0.05 or less rejects the null hypothesis at the 5% level, that is, only 5% of the probability the supposed statistical model will fail to predict the response. The *p*-values less than 0.05 indicate that model terms are significant and in this case *C* and *H* are significant model terms. Lack of fit (LOF) is a special investigative test for adequacy of a model fit. If the model does not fit the data well, this will be significant. The LOF *F*-value of 47.70 implies that the LOF is not significant relative to the pure error. There is only 8.33% chance that a large LOF *F*-value of 47.7 could occur due to noise. The model adequacies were checked by the determination coefficients (R^2), adjusted R^2 (adj-R^2), and predicted R^2 (pred-R^2). The R^2 is a measure of how well the regression equation fits the sample data. The adj-R^2 is a modification of R^2 that adjusts for the number of explanatory terms in a model. A pred-R^2 is used to measure the amount of variation in new data explained by the model. The pred-R^2 and the adj-R^2 should be within 0.20 of each other. Otherwise there may be a problem with either the data or the model. Here, the obtained values for adj-R^2 and pred-R^2 are 0.8392 and 0.7744, respectively. The pred-R^2 of 0.8392 is in reasonable agreement with the adj-R^2 of 0.7744 and it might be also said that the R^2 of 0.8676 was in reasonable agreement with the experimental results, indicating that 86.76% of the variability could be revealed by the model. Adequate precision measures the signal to noise ratio and a ratio greater than 4.0 is desirable. Here, a value of 4.717 for adequate precision indicates an adequate signal and this model can be used to navigate the design space.

According to the results of ANOVA for R_2 (Table 4), the model *F*-value of 26.47 implies that the model is significant and there is only a 0.01% chance that a large model *F*-value of 26.47 could occur due to noise. According to *p*-values, *E*, *F* and *G* are significant model terms. The LOF's *F*-value of 17.43 implies the LOF is not significant relative to the pure error. There is a 1.6% chance that a large LOF's *F*-value could occur due to noise. The obtained values for adj-R^2 and pred-R^2 were 0.9206 and 0.8858, respectively. The pred-R^2 is in reasonable agreement with the adj-R^2 and it might be also said that the R^2 of 0.9486 was in reasonable agreement with the experimental results, indicating 94.86% of the variability could be revealed by the model. Here, a value of 13.698 for adequate precision indicates an adequate signal and this model can be used to navigate the design space.

On the other hand, in order to get a deeper insight, diagnostic plots (half-normal plot and standardized Pareto chart) for both analyzed responses were built, which allowed us to reach a similar conclusion. The half-normal plots of effects of variables on responses are shown in Fig. 1. Fig. 1A reveals two main effects from factors *H* and *C* on the R_1 while, Fig. 1B reveals three main effects from factors *E*, *F* and *G* on R_2. The other (unlabeled) effects line up normally near low levels of effect and, in all likelihood, they vary because of experimental error [37].

Standardized Pareto charts represent the estimated effects of variables and variables' interactions on responses. In order to determine the importance of the significant variables, standardized Pareto charts (Fig. 2) were employed. To make the Pareto chart more robust to experimental mishaps, it has been plotted with the *t*-values of the effects. A more conservative *t*-value (Bonferroni limit) [37], takes the number of estimated effects into account by dividing it into the desired probability for the risk value [37]. These two values of *t*-test can help us to distinguish the significant variables from insignificant ones. The most significant effects were towering over the Bonferroni limit, the significant effects towering above the *t*-value limit, and the insignificant effects towering under the *t*-value limit, Fig. 2A–B.

Therefore, as a conclusion of the screening step, *C*, *E*, *F*, *G* and *H* variables must be considered as key variables affecting the responses in the further optimization analysis. The other variables were detected as insignificant variables and were held constant at their respective optimal levels throughout all the experiments.

3.2. Developing mathematical models by FCCCD

By the use of FCCCD two models were developed. In each model, the variables were evaluated by ANOVA and a backward regression procedure was applied to eliminate the insignificant ones. The obtained results are shown in Table 5. As can be seen for R_1, the *p*-value of LOF was found to be 0.9763 and indicates that the model fitted the response well. The model *F*-value of 5.58 implies that the model is significant. There is only a 0.01% chance that a large *F*-value of 5.58 could occur due to noise. The pred-R^2 of 0.7546 was in reasonable agreement with

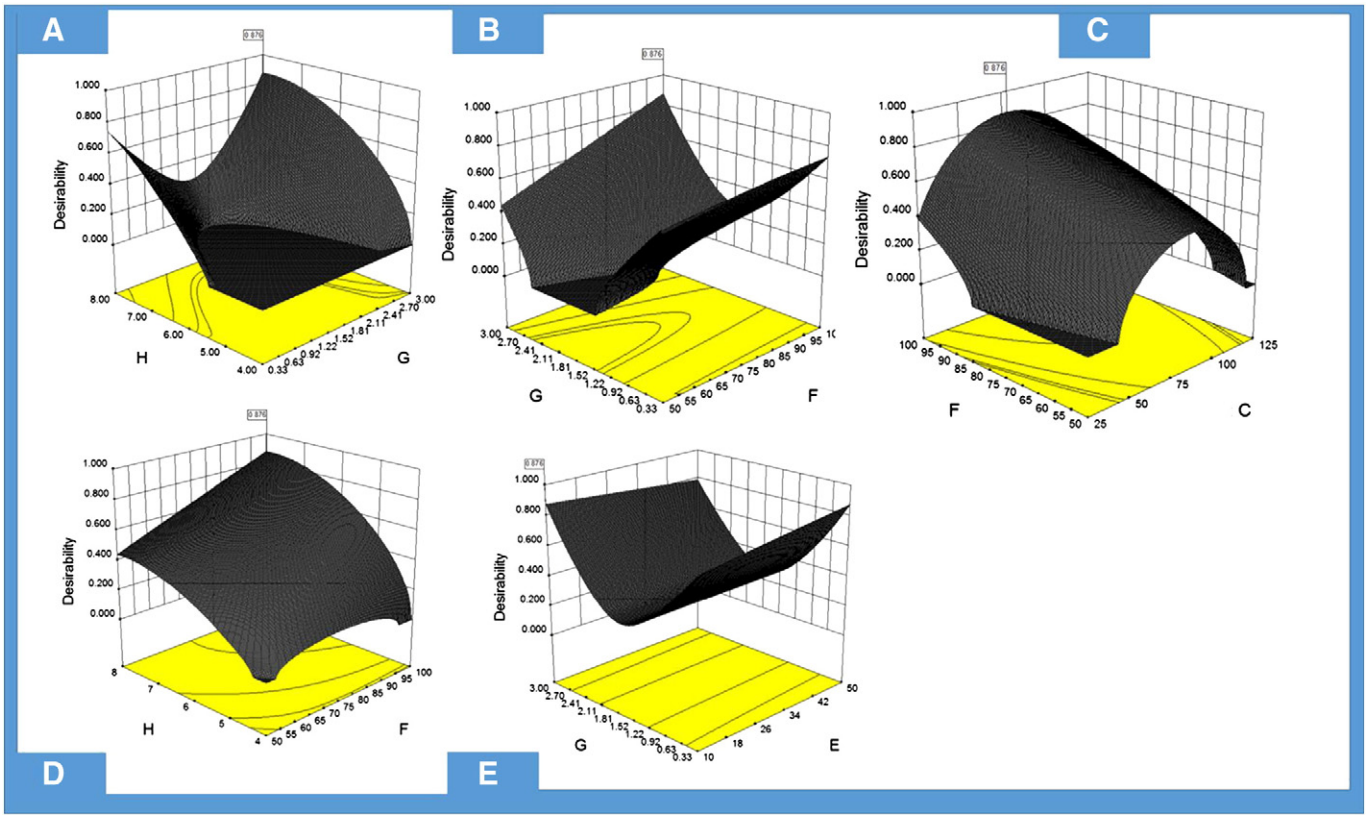

Fig. 3. Response surface plots corresponding to the DF when optimizing the following pair of variables, while maintaining constant the remaining ones at their optimum values: (A) *H-G*; C = 75 cycles, $E = 10$ cycles, and $F = 100$ mV s^{-1} (B) *G-F*; $C = 75$ cycles, $E = 10$ cycles, and $H = 7.98$ (C) *F-C*; $E = 10$ cycles, $G = 3$ and $H = 7.98$ (D) *H-F*; $C = 75$ cycles, $E = 10$ cycles, and $G = 3$ (E) *G-E*; $C = 75$ cycles, $F = 100$ mV s^{-1}, and $H = 7.98$.

the adj-R^2 of 0.8167 and it might be also said that the R^2 of 0.8435 was in reasonable agreement with the experimental results. A value of 7.911 for adequate precision indicates an adequate signal and this model can be used to navigate the design space.

According to the results of Box–Cox plot (not shown) a square root transformation was chosen as the best possible transformation for R_1. This plot provides a guideline for selecting the correct power (lambda) law transformation [44]. A recommended transformation is listed, based on the best lambda value, which is found at the minimum point of the curve generated by the natural log of the sum of squares of the residuals.

The polynomial model for R_1 was obtained by considering the significant terms and was expressed by:

$$\begin{aligned}\sqrt{R_1} = &-4.70738 \times 10^{-4} + 1.44409 \times 10^{-4}C - 1.63163 \\ &\times 10^{-5}\ F - 5.09710 \times 10^{-3}G + 1.20182 \times 10^{-3}H \\ &+ 1.94522 \times 10^{-5}FG - 2.80796 \times 10^{-4}\mathrm{GH} - 9.01477 \\ &\times 10^{-7}C^2 + 1.63400 \times 10^{-3}G^2.\end{aligned} \tag{5}$$

The statistical significance of the polynomial model was checked by *F*-test, and as can be seen the *p*-value is less than 0.01% which confirms that the model is highly significant. The model reveals that *H* and G^2 had significant effects on R_1 as they had the larger coefficient. Positive coefficient of *H* and *C* and quadratic terms *FG* and G^2 indicated a linear effect to increase. However, *F*, *G* and quadratic terms *GH* and C^2 had negative effects.

Table 5 shows the results of ANOVA for R_2 as well. As can be seen, the LOF's *p*-value of 0.6322 indicates that the model fits the response well. The model *F*-value of 0.89 implies that the model is significant. The pred-R^2 of 0.7554 was in reasonable agreement with the adj-R^2 of 0.8036 and it might be also said that the R^2 of 0.8334 was in reasonable agreement with the experimental results. A value of 15 for adequate precision indicates an adequate signal and this model can be used to navigate the design space. The polynomial model for R_2 was expressed by:

$$\begin{aligned}R_2 = &\ 0.90690 - 3.58676 \times 10^{-4}C - 2.77452 \times 10^{-4}E + 1.14118 \\ &\times 10^{-4}F - 0.019885G\text{-}0.045299H + 4.5 \times 10^{-6}\mathrm{CF} + 1.42790 \\ &\times 10^{-4}EG - 7.62500 \times 10^{-5}FH + 1.94288 \times 10^{-3}GH \\ &+ 3.25882 \times 10^{-3}H^2\end{aligned} \tag{6}$$

The statistical significance of the polynomial model was checked by *F*-test, and as can be seen the *p*-value is less than 0.01% which indicated that the model is highly significant.

After building the mathematical models with good statistical characteristics, optimization of the procedure and finding the optimal levels of the significant variables would be started in the next section.

3.3. Simultaneous optimization by Derringer's desirability function

It is not possible by a simple visual inspection of the response surfaces obtained with the fitted models, to find out the experimental conditions (variables' levels) to reach simultaneously the optimal value for all the evaluated variables. In such cases, the DF allows to obtain these parameters including, moreover, the researcher's priorities during the optimization procedure [45,46]. At the first step, a partial desirability function for each individual response was created using the fitted models and establishing the optimization criteria for each one. Variables' levels were also included in the optimization procedure, in order to prioritize the use of certain suitable conditions within the

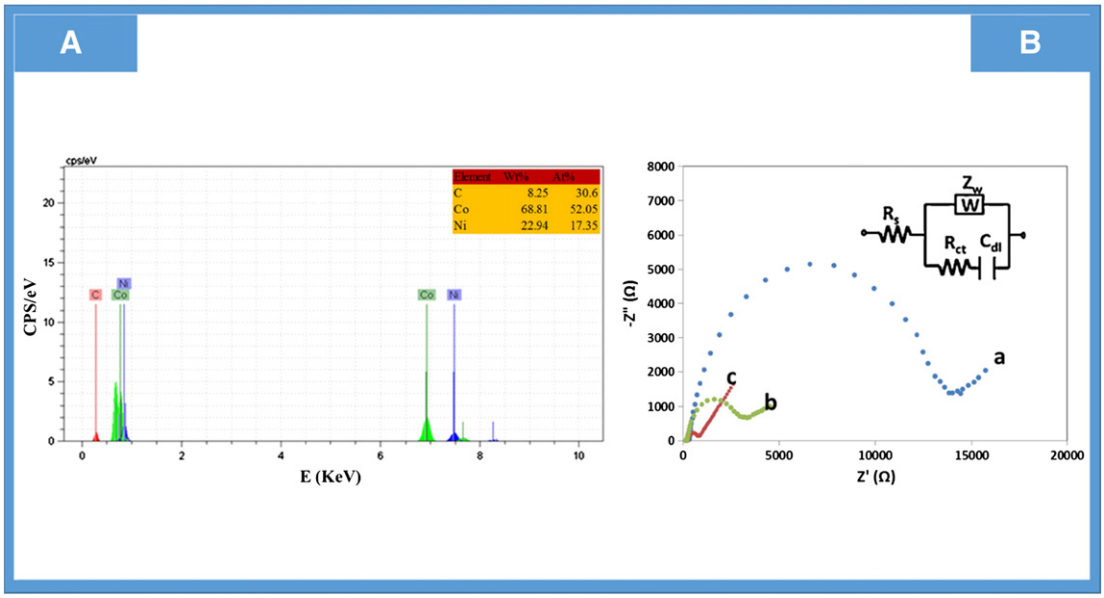

Fig. 4. (A) The EDS spectra of CoNi NPs/ERGO nanocomposite. Inset shows the weight and atomic percentages of C, Co, and Ni in the nanocomposite. (B) The EIS spectra of (a) bare GCE, (b) ERGO modified GCE, and (c) CoNi NPs/ERGO modified GCE in 1.0 M KCl containing 5.0 mM $K_4[Fe(CN)_6]/K_3[Fe(CN)_6]$. The inset shows equivalent circuit $R_s([R_{ct}C_{dl}]Z_w)$. R_s: solution resistance, R_{ct}: electron transfer resistance, C_{dl}: double layer capacitance, Z_w: Warburg impedance.

experimental region. The most desirable ranges for each design variable or response were selected, deciding if these responses or variables had to be maximized (R_1 and F), minimized (R_2) or maintained in the range (C, E, G and H). In addition, a weight or emphasis was given to each goal. The importance may vary from 1.0 for the least important variable to 5.0 for the most important one. After that, the global DF was obtained using the Eq. (4). Apart from optimizing the responses to reach a suitable CV of nitrite, we also attempted to maximize F to

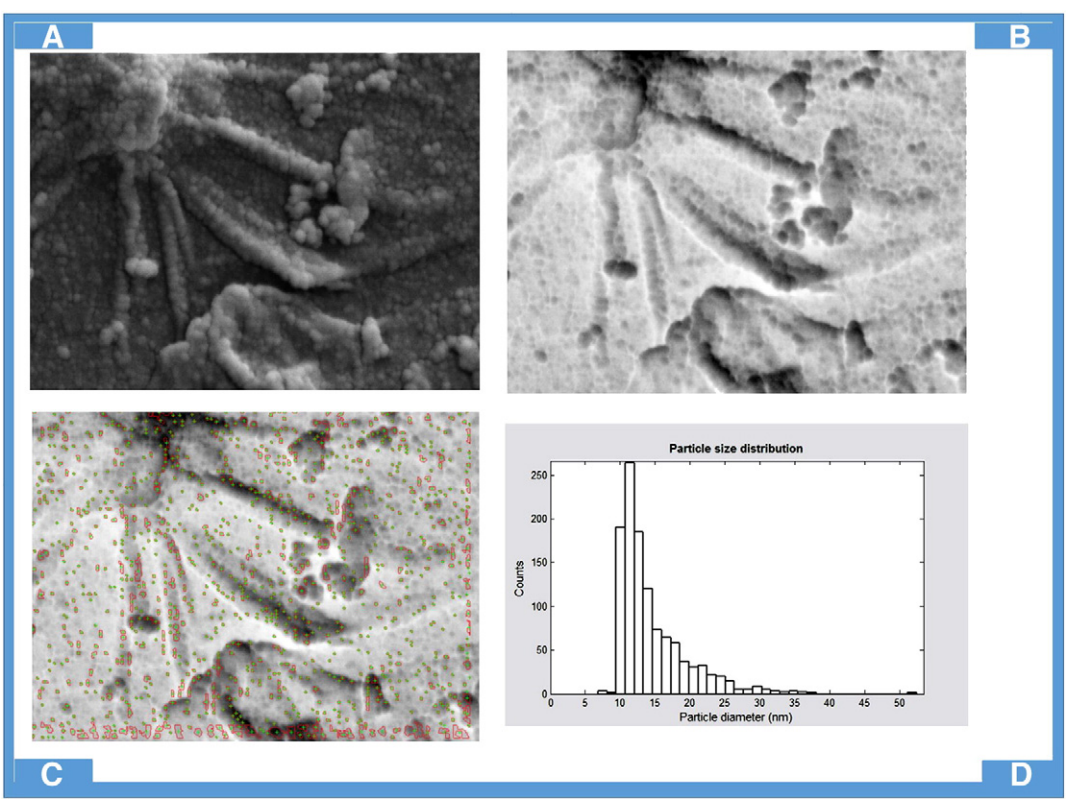

Fig. 5. (A) The original SEM image of CoNi NPs/ERGO/GCE, (B) the contrast of the original SEM image for detecting NPs, (C) detected NPs marked by pluses and surrounded by red circles, and (D) a plot representing the PSDs.

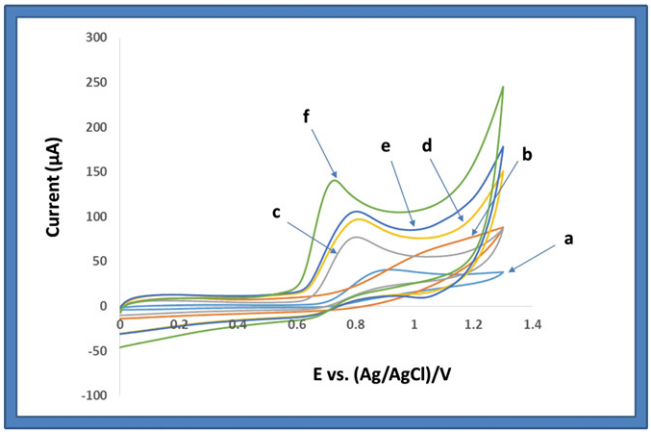

Fig. 6. The CVs obtained at (a) bare GCE, (b) GO/GCE, (c) ERGO/GCE, (d) Ni NPs/ERGO/GCE, (e) Co NPs/ERGO/GCE and (f) CoNi NPs/ERGO/GCE under the identified optimal level of the variables in 0.05 M PBS (pH = 7.98) containing 1.0 mM nitrite at the scan rate of 0.05 V s^{-1}.

reduce the time of fabrication. Following the conditions and restrictions previously discussed, the optimization procedure was carried out and the response surfaces obtained for the global DF are presented in Fig. 3A–E. These plots were obtained for a given pair of variables, while maintaining the other three fixed at their optimal values. Finally, the values of the variables which maximize R_1 and minimize R_2 have been chosen as the optimal experimental conditions. They resulted in $C = 75$ cycles, $E = 10$ cycles, $F = 100$ mV/s, $G = 3$, and $H = 7.98$. The global desirability resulted in 0.877; which could be considered as highly acceptable taking into account the large number of variables being simultaneously optimized.

3.4. Verification of the model

Under the optimal conditions, the predicted values of R_1 and R_2 were 0.00013868 A and 0.6987 V, respectively. With triplicate experiments, the mean values of R_1 and R_2 were $(1.51 \pm 0.21) \times 10^{-4}$ A and 0.715 $\pm$ 0.021 V, respectively, which are in an excellent agreement with the predicted ones. As a result, the computed models were considered to be accurate and reliable for predicting the R_1 and R_2.

3.5. Characterizations of CoNi NPs/ERGO nanocomposite

Elemental compositions of CoNi NPs/ERGO nanocomposite were analyzed by EDS (Fig. 4 A). Signature peaks for C, Co and Ni were observed for CoNi NPs/ERGO nanocomposite. The weight percentage of C, Co, and Ni in the nanocomposite was 8.25%, 68.81% and 22.94%, respectively. This corresponded well to the molar ratio of metal precursors and indicated Co and Ni can both be successfully electrochemically synthesized under the given conditions and contribute [Co]/[Ni] = 3.0 towards formation of bimetallic NPs during the synthesis.

The EIS is a useful tool to monitor modifications step-by-step using $[Fe(CN)_6]^{4-/3-}$ redox couple as electrochemical probe (Fig. 4 B). As GCE was modified with ERGO (curve b), the charge transfer resistance (R_{ct}) drastically decreased compared to that of bare GCE (curve a). This implied ERGO formed an interpenetrating network in favor of diffusion of redox probes and interfacial electron transfers. R_{ct} continued to decrease as ERGO was further modified with CoNi bimetallic alloy NPs (curve c). As expected, the decrease of charge transfer resistance value for CoNi NPs/ERGO nanocomposite is due to acting these NPs as conductive shreds and increasing the porous microcrystalline structure of ERGO randomly ordered to improve electron transfer kinetic.

The surface morphologies of CoNi NPs/ERGO nanocomposite were characterized by SEM, Fig. 5A. In order to provide statistically meaningful PSDs from SEM images, many particles should be analyzed. Manual segmentation of SEM images can be time-consuming because, in most cases, it is difficult to analyze an image locally to obtain only the desired information from the particles. Therefore, we have applied DIP for processing and extracting meaningful information from the original SEM image. Briefly, the original SEM image (Fig. 5 A) was processed for detecting NPs using a semiautomatic segmentation including interactive selection of particles, binarisation with adaptive thresholding (Otsu's method) and finally deleting those particles that did not seem good, Fig. 5B. Then this image was used for particle counting and average diameter measurement. The DIP detected 1150.0 NPs marked by pluses

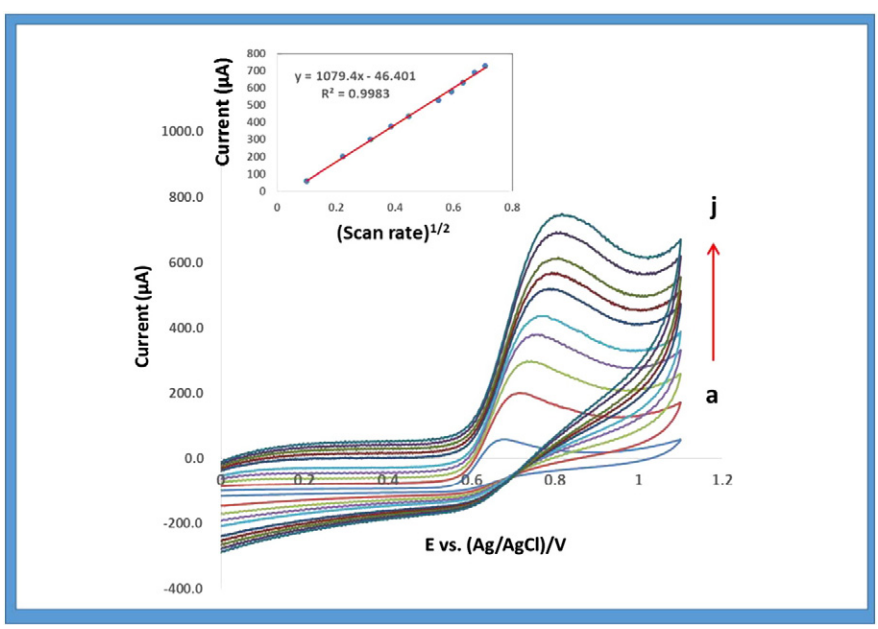

Fig. 7. The CVs of CoNi NPs/ERGO/GCE at different scan rates in 0.05 M PBS (pH 7.98) containing 0.1 mM nitrite. Inner to outer are (a) 0.01, (b) 0.05, (c) 0.10, (d) 0.15, (e) 0.20, (f) 0.30, (g) 0.35, (h) 0.40, (i) 0.45 and (j) 0.50 V s^{-1}. The inset shown above is I_p vs. (scan rate)$^{1/2}$.

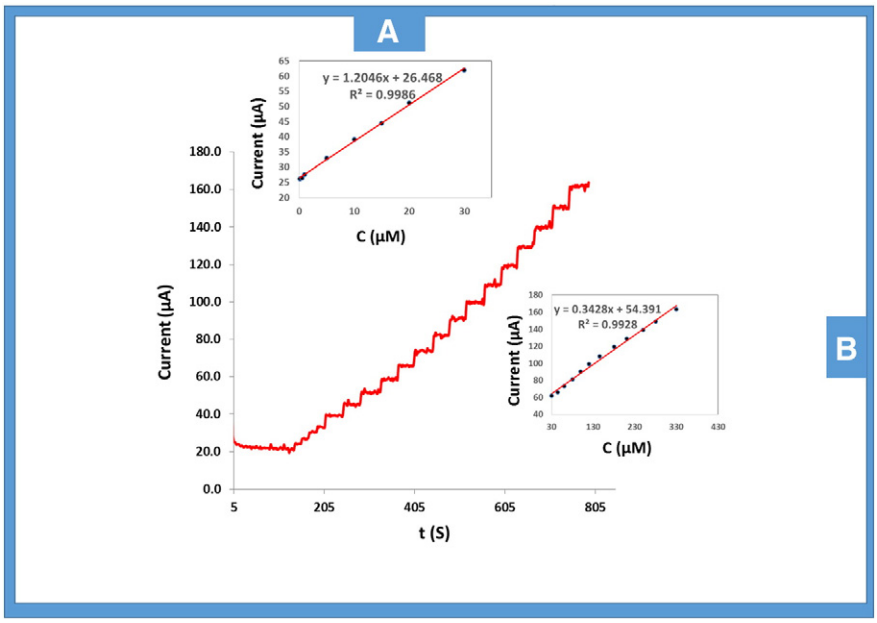

Fig. 8. Amperometric response at CoNi NPs/ERGO modified rotating disk GCE upon successive additions of nitrite (0.1–330.0 μM) into gently stirred 0.05 M PBS (pH 7.98), $E_{app} = +0.715$ V. Insets (A) and (B) are the linear calibration plots of response currents (μA) vs. concentration ranges of 0.1–30.0 μM and 30.0–330.0 μM nitrite, respectively.

and surrounded by red circles, Fig. 5C–D shows the PSDs which confirms a mean diameter of 15.0 ± 4.9 nm, a maximum size of 52.0 nm, and a minimum size of 6.8 nm. Also the results of DIP confirmed that the ERGO was modified with homogeneously dispersed CoNi bimetallic alloy NPs in a good size distribution having suitable density (6.76×10^4 NPs/cm^2, computed from a 0.017 cm^2 GCE surface analysis).

3.6. Analytical characterization

Fig. 6 shows the CVs obtained at (a) bare GCE, (b) GO, (c) ERGO, (d) Ni NPs/ERGO, (e) Co NPs/ERGO and (f) CoNi NPs/ERGO modified GCEs in the presence of 1.0 mM nitrite under the identified optimal level of the variables. CoNi NPs/ERGO modified GCE shows well defined, enhanced nitrite oxidation peak at +0.71 V. It is worth noting that, this oxidation peak potential was roughly 190.0 mV less positive than unmodified GCE. Moreover, nitrite oxidation peak current noticed at CoNi NPs/ERGO modified GCE was 3.72 fold higher than that of unmodified GCE. Both decrease in overpotential and enhancement in catalytic oxidation current indicate its promising catalytic activity towards nitrite. This superior catalytic performance of CoNi NPs/ERGO was attributed to the larger surface area, more electroactive sites, faster electron transfer kinetics and the interpenetrating low-resistance 2-D network of ERGO, favorable for dispersion and nucleation of CoNi bimetallic alloy NPs, however we cannot neglect the excellent performance of ED in optimization of the procedure.

Fig. 7, (a–j) shows the effect of scan rate on CoNi NPs/ERGO modified GCE. The anodic oxidation peak current increased linearly with square root of scan rates (inset of Fig. 7), indicating a diffusion controlled process. As reported by Guidelli et al. the nitrite oxidation is a second-order homogeneous disproportionation process [47]. The overall reaction can be expressed as follows:

$$NO_2^- + H_2O \rightarrow NO_3^- + 2H^+ + 2e. \quad (7)$$

Thus it is evident from the Eq. (7), NO_3^- is the only plausible final product.

Since amperometry under stirred conditions has a much higher current sensitivity than cyclic voltammetry, it was used to estimate the lower LOD. Fig. 8 displays typical amperogram obtained at the CoNi NPs/ERGO modified GCE with successive injection of nitrite into continuously stirred PBS (0.05 M, pH 7.98) at an applied potential of 0.71 V vs. Ag/AgCl (sat'd) electrode. As shown, during the successive addition of nitrite a well-defined response was observed. The response current is linear in the nitrite concentration ranges of 0.1–30 μM (inset A of Fig. 8) and 30–330 μM (inset B of Fig. 8). The LOD (S/N = 3) using the formula: LOD = $3.0S_b/S$ (S_b: standard deviation of blank signal and S: analytical sensitivity) was found to be 0.05 μM. Therefore, according to the calculated LOD it can be concluded that the CoNi NPs/ERGO modified GCE is highly sensitive.

3.7. Interference study

The effects of some possible interfering substances were studied prior to the application of the proposed sensor for the assay of nitrite in real samples. The anti-interference ability of the CoNi NPs/ERGO modified GCE was investigated by adding various interferences into a 0.05 M PBS (pH 7.98) containing 50 μM nitrite. It was found that 150-folds Ca^{2+}, Mg^{2+}, Ni^{2+}, Cu^{2+}, Al^{3+}, SO_3^{2-}, CO_3^{2-}, SO_4^{2-}, Na^+, K^+ and HSO_4^-; 200-folds H_2O_2; 20-folds glucose and $CuSO_4$; 100-folds dopamine, uric acid and ascorbic acid did not give any significant interference on the response of the CoNi NPs/ERGO modified GCE. Thus, this study reveals that the developed sensor can tolerate a high concentration of interfering substances and, therefore, can be stated as highly selective in the presence of the more common interfering substances.

3.8. Repeatability, reproducibility, stability and analytical application

The repeatability and reproducibility of the proposed sensor were evaluated using differential pulse voltammetry. The repeatability of one electrode to determine 50.0 μM nitrite was fairly good. The relative standard deviation (RSD) was 0.95% for 8.0 successive assays. The electrode-to-electrode reproducibility was estimated from the response to 50.0 μM nitrite with 7.0 different sensors and this series yielded a RSD of 4.45%. The obtained results confirmed good repeatability and reproducibility of the proposed sensor. Such good repeatability and reproducibility of this sensor can be due to the less fouling effect of the CoNi NPs/ERGO modified GCE. In addition, long-term stability was investigated by

Table 6
Comparison of the fabricated sensor with other reported sensors for nitrite.

Electrode	Method	Peak potential (V)	Linear range (μM)	LOD (μM)	Ref.
TiO_2 sol–gel/Aunano/Hb[a]/GCE	Amperometry	0.75	4–350	1.2	[48]
Nano-Pt/P3MT[b]/GCE	DPV	0.77	5–170	1.5	[49]
Pt/PI[c]/CNTs[d]	DPV	0.93	500–7000	5	[50]
Au–Pt NPs/ITO	LSV	0.79	2.5–40	1	[51]
CR[e]-GO/GCE	Amperometry	0.80	8.9–167	1	[31]
PtNPs/ITO[f]	Amperometry	0.70	5–800	0.4	[52]
CPE modified with CoHCF[g]	Amperometry	0.92	0.1–2.15 mM	1.19	[53]
PtNPs/DPAN[h]/Au	Amperometry	−0.3	10–1000	5	[54]
Au NPs/SG[i]/GCE	Amperometry	0.77	10–3.96 mM	0.2	[55]
Gr[j]/PP[k]/CT[l]/GCE	Amperometry	0.73	0.5–722	0.5	[56]
CoNi NPs/ERGO/GCE	Amperometry	0.71	0.10–30 and 30–330	0.05	This work

[a] Hemoglobin.
[b] Poly(3-methylthiophene).
[c] Aromatic polyimide.
[d] Carbon nanotubes.
[e] Chemically reduced.
[f] Indium tin oxide.
[g] Cobalt hexacyanoferrate.
[h] 5-[1,2]Dithiolan-3-yl-pentanoic acid [2-(naphthalene-1-ylamino)-ethyl]amide.
[i] Solfonated graphene.
[j] Graphene.
[k] Ploy pyrrole.
[l] Chitosan.

measuring nitrite concentration for one month. In dry conditions, current response of the proposed sensor was maintained at 93.0% after one month, whereas only 72.0% remained in wet conditions by keeping the sensor in a humid place. Findings indicated that the sensor should be stored in dry conditions for long-term use. Such a good performance might be attributed to the fact that CoNi NPs/ERGO composite is firmly attached onto the surface of GCE.

The obtained results by the proposed sensor with some reported sensors [31,48–56] for the determination of nitrite were compared and given in Table 6. The proposed sensor provides better results over the most of the reported electrodes.

The sensor was applied for nitrite determination in several foodstuffs and water samples by amperometry and the obtained results are presented in Table 7.

Results on the nitrite content in the analyzed real samples were compared with those obtained from the Griess protocol [57]. The results from the sensor were similar to those obtained by the Griess method, validating its suitability as a novel nanocomposite material for nitrite determination.

4. Conclusion

In this study, a highly efficient optimization procedure based on the statistical methodology by combining Min-Run Res IV FD, face centered central composite design and desirability function was developed and demonstrated to be effective and reliable in selecting the statistically significant variables and optimizing their levels. A simple, controllable, computationally designed, fast, convenient and green approach was proposed to synthesize CoNi NPs/ERGO nanocomposite. The SEM image of the modified electrode was processed by DIP and the obtained results confirmed that the ERGO has been modified with homogeneously dispersed CoNi bimetallic alloy NPs in a good size distribution having suitable density. The prepared sensor exhibits a high sensitivity, high selectivity, good stability, acceptable repeatability and reproducibility, and can be successfully applied in determination of nitrite in different real samples. The sensor was computationally designed and characterized to introduce a new and advanced field in electrochemistry and without any exaggeration this study is unique among the reported works in constructing electrochemical sensors and definitely could produce a great base for more interesting studies in near future.

Table 7
Content of nitrite in real samples determined by the proposed and Griess methods.

Sample	Detected	
	This work	Griess method
Damavand mineral water (mg/mL)	0.20 ± 0.03[a]	0.19 ± 0.02[a]
Hot dog sausage (mg/g)	31.08 ± 0.51	32.65 ± 0.21
Mortadella salami (mg/g)	26.77 ± 0.11	26.98 ± 0.33
Feta white cheese (mg/g)	4.38 ± 0.49	4.66 ± 0.16

[a] Mean value ± standard deviation.

Acknowledgment

We wish to express our sincere appreciation to Razi University Research Council, UNL, CONICET and ANPCyT for providing us fund and time to this project. We would also like to thank the reviewers for their insightful comments which led us to an improvement of the work.

References

[1] N. Spătaru, T.N. Rao, D.A. Tryk, A. Fujishima, J. Electrochem. Soc. 148 (2001) 112–117.
[2] A. Amine, G. Palleschi, Anal. Lett. 37 (2004) 1–19.
[3] W. Lijinsky, S.S. Epstein, Nature 225 (1970) 21–23.
[4] S.S. Mirvish, Cancer Lett. 93 (1995) 17–48.
[5] V.V. Kuznetsov, S.V. Zemyatova, J. Anal. Chem. 62 (2007) 637–644.
[6] H. Takiguchi, A. Tsubata, M. Miyata, T. Odake, H. Hotta, T. Umemura, K. Tsunoda, Anal. Sci. 22 (2006) 1017–1019.
[7] B. Prusisz, L. Jaskiewicz, P. Pohl, Microchim. Acta 156 (2006) 219–223.
[8] P. Niedzielski, I. Kurzyca, J. Siepak, Anal. Chim. Acta. 577 (2006) 220–224.
[9] T. Miyado, Y. Tanaka, H. Nagai, S. Takeda, K. Saito, K. Fukushi, Y. Yoshida, O. Nadzhafova, M. Etienne, A. Walcarius, Electrochem. Commun. 9 (2007) 1189–1195.
[10] A. Lagalante, P. Greenbacker, Anal. Chim. Acta. 590 (2007) 151–158.
[11] B. Strehlitz, B. Grundig, W. Schumacher, P.M.H. Kroneck, K.D. Vorlop, H. Kotte, Anal. Chem. 68 (1996) 807–816.
[12] L.H. Larsen, L.R. Damgaard, T. Kjaer, T. Stenstrom, A. Lynggard-Jensen, P. Revsbech, Water Res. 34 (2000) 2458–2461.
[13] S.Q. Liu, H.X. Ju, Analyst 128 (2003) 1420–1424.
[14] A.K. Geim, K.S. Novoselov, Nat. Mater. 6 (2007) 183–191.
[15] S. Stankovich, D.A. Dikin, G.H.B. Dommett, K.M. Kohlhaas, E.J. Zimney, R.D. Piner, S.T. Nguyen, R.S. Ruoff, Nature 442 (2006) 282–286.
[16] R. Muszynski, B. Seger, P.V. Kamat, J. Phys. Chem. C 112 (2008) 5263–5266.
[17] X. Kang, J. Wang, H. Wu, I.A. Aksay, J. Liu, Y. Lin, Biosens. Bioelectron. 25 (2009) 901–905.
[18] S.L. Chou, J.Z. Wang, M. Choucair, H.K. Liu, J.A. Stride, S.X. Dou, Electrochem. Commun. 12 (2010) 303–306.
[19] M.D. Stoller, S. Park, Y. Zhu, J. An, R.S. Ruoff, Nano Lett. 89 (2008) 3498–34502.
[20] J. Lu, I. Do, L.T. Drzal, R.M. Worden, I. Lee, ACS Nano 2 (2008) 1825–1832.

[21] B.G. Choi, H. Park, T.J. Park, M.H. Yang, J.S. Kim, S.Y. Jang, N.S. Heo, S.Y. Lee, J. Kong, W. H. Hong, ACS Nano 4 (2010) 2910–2918.
[22] J. Yang, W.D. Zhang, S. Gunasekaran, Biosens. Bioelectron. 26 (2010) 279–284.
[23] A. Safavi, F. Farjami, Biosens. Bioelectron. 26 (2011) 2547–2552.
[24] J.C. Claussen, A.D. Franklin, A. ul Haque, D.M. Porterfield, T.S. Fisher, ACS Nano 3 (2009) 37–44.
[25] N. Lopez, T.V.W. Janssens, B.S. Clausen, Y. Xu, M. Mavrikakis, T. Bligaard, J.K. Nørskov, J. Catal. 223 (2004) 232–235.
[26] V.M. Morris, C. Hargreaves, K. Overall, P.J. Marriott, J.G. Hughes, J. Chromatogr. A 766 (1997) 245–254.
[27] R.G. Brereton, Chemometrics Data Analysis for the Laboratory and Chemical Plant, John Wiley, Wiltshire, 2004.
[28] N. Costa, A. Pires, C. Ribeiro, Total Qual. Manag. Mag. 18 (2006) 386–391.
[29] R. Myers, D. Montgomery, C. Anderson-Cook, Response Surface Methodology: Process and Product Optimization Using Designed Experiments, John Wiley, New Jersey, 2008.
[30] M. Tanco, E. Viles, L. Ilzarbe, M. Alvarez, Appl. Stoch. Model. Data Anal. 25 (2009) 478–505.
[31] V. Mani, A.P. Periasamy, S.M. Chen, Electrochem. Commun. 17 (2012) 75–78.
[32] W.S. Hummers, R.E. Offeman, J. Am. Chem. Soc. 80 (1958) 1339–1342.
[33] Y. Xu, H. Bai, G. Lu, C. Li, G. Shi, J. Am. Chem. Soc. 130 (2008) 5856–5857.
[34] M.M. De Zan, M.D. Gil García, M.J. Culzoni, R.G. Siano, H.C. Goicoechea, M. Martínez Galera, J. Chromatogr. A 1179 (2008) 106–114.
[35] P.H.C. Eilers, I.D. Currie, M. Durban, Comput. Stat. Data Anal. 50 (2006) 61–67.
[36] P.H.C. Eilers, Anal. Chem. 76 (2004) 404–411.
[37] M.J. Anderson, P.J. Whitcomb, DOE Simplified: Practical tools for effective experimentation, Productivity Press, New York, 2007.
[38] B. Dejaegher, Y. Vander Heiden, Acta Chromatogr. 21 (2009) 161–170.
[39] A.M. Carro, I. Neira, R. Rodil, R.A. Lorenzo, Chromatographia 56 (2002) 733–738.
[40] M.E. Rueda, L.A. Sarabia, A. Herrero, M.C. Ortiz, Anal. Chim. Acta. 479 (2003) 173–184.
[41] E. Rueda, M.C. Ortiz, L.A. Sarabia, A. Herrero, Anal. Chim. Acta. 498 (2003) 119–125.
[42] M.J. S'aiz-Abajo, J.M. Gonz'alez-S'aiz, C. Pizarro, Anal. Chim. Acta. 528 (2005) 63–76.
[43] M.C. Ortiz, A. Herrero, S. Sanllorente, C. Reguera, Talanta 65 (2005) 246–254.
[44] M.J. Anderson, P.J. Whitcomb, RSM Simplified: Optimizing processes using response surface methods for design of experiments, Productivity Press, New York, 2005.
[45] M. Almeida Bezerra, R. Erthal Santelli, E. Padua Oliveira, L. Silveira Villar, L.A. Escaleira, Talanta 76 (2008) 965–977.
[46] L. Vera Candioti, J.C. Robles, V.E. Mantovani, H.C. Goicoechea, Talanta 69 (2006) 140–147.
[47] R. Guidelli, F. Pergola, G. Raspi, Anal. Chem. 44 (1972) 745–755.
[48] W. Yang, Y. Bai, Y. Li, C. Sun, Anal. Biochem. 382 (2005) 44–51.
[49] Y. Zhou, H. Xian, F. Li, S. Wu, Q. Lu, Y. Li, L. Wang, Electrochim. Acta 55 (2010) 5905–5910.
[50] X. Zhang, X. Shi, C. Wang, Catal. Commun. 10 (2009) 610–616.
[51] Y. Song, Y. Ma, Y. Wang, J. Di, Y. Tu, Electrochim. Acta 55 (2010) 4909–4914.
[52] F. Liang, M. Jia, J. Hu, Electrochim. Acta 75 (2012) 414–421.
[53] H. Heli, I. Eskandari, N. Sattarahmady, A.A. Moosavi-Movahedi, Electrochim. Acta 77 (2012) 294–301.
[54] P. Miao, M. Shen, L. Ning, G. Chen, Y. Yin, Anal. Biochem. 399 (2011) 2407–2411.
[55] S.J. Li, G.-Y. Zhao, R.-X. Zhang, Y.-L. Hou, L. Liu, H. Pang, Microchim. Acta 180 (2013) 821–827.
[56] D. Ye, L. Luo, Y. Ding, Q. Chena, X. Liua, Analyst 136 (2011) 4563–4569.
[57] Analytical methods committee, Analyst 112 (1987) 199–204.